

The Significance of the Critical Stress Ratio in the Formulation of Nonlinear Constant Life Diagrams for CFRP Laminate Life Prediction

Alok Behera¹  · Sandeep Kale² ·
Manjusha M. Thawre² · Atul Ballal²

Received: 20 August 2023 / Accepted: 24 June 2024
© The Institution of Engineers (India) 2024

Abstract The constant life diagram (CLD), a trusted method for life prediction, is generated based on static strength and constant amplitude fatigue data. This study examines the predictive accuracy of various nonlinear CLDs, including the innovative Anisomorphic CLDs, for a [+ 45, - 45]_{3S} carbon fiber reinforced polymer composite laminate fabricated via autoclave curing with a 59% fiber volume. Initial calculations encompassed ultimate tensile strength (UTS) and ultimate compressive strength (UCS) using a constant crosshead speed of 1 mm/min. Subsequently, constant amplitude fatigue experiments were conducted for five stress ratios, encompassing the critical stress ratio (CSR) ($\chi = \text{UCS/UTS}$), $R = 0.1$ and 0.5 (tension–tension), -1 (tension–compression), and 5 (compression–compression). The predictive accuracy of three top-performing nonlinear CLDs, i.e., asymmetric Gerber, inclined Goodman, and the innovative Anisomorphic CLD, was assessed through necessary stress–life (S – N) curves. Notably, the novel Anisomorphic CLD, utilizing only static and CSR fatigue data, demonstrated optimal accuracy, positioning the maximum amplitude stress for any random fatigue life (N_f) on CSR. Its practical implementation undoubtedly streamlines the process, saving time, money, and effort required for extensive fatigue data generation.

Keywords CLD · Multidirectional · Life prediction · Critical stress ratio · Fatigue

✉ Alok Behera
alokbeheraphd@gmail.com

¹ Department of Mechanical Engineering, Indian Institute of Science, Bangalore, Karnataka, India

² Department of Metallurgical and Materials Engineering, Visvesvaraya National Institute of Technology, Nagpur, India

Introduction

Polymer matrix composites (PMCs) have efficiently served several structural applications for over half a century. However, scientists still hesitate to replace the traditional material with PMCs due to its complexity, anisotropy, the absence of universal failure theory, and commonly accepted life prediction tool. Structures used in aircraft or wind turbine blades are vulnerable to cyclic stress because the live load is greater than the dead load [1]. Common issues plague PMCs, including susceptibility to moisture ingress [2–8], resulting mechanical property degradation [9–13], inadequate resistance against sliding wear [14–17], and vulnerability to dynamic loading conditions [18–21]. Moisture ingress is a persistent concern, compromising structural integrity and triggering a gradual decline in mechanical properties. Moreover, PMCs often exhibit insufficient resistance to sliding wear, heightening the risk of surface damage and material deterioration over time. The weakness against dynamic loading conditions further underscores the need for robust material formulations and engineering solutions to enhance resilience under varying stress environments. Addressing these multifaceted challenges necessitates a nuanced understanding of composite behavior and the development of innovative strategies to bolster resistance to moisture, wear, and dynamic loads. Consequently, ongoing research and advancements in composite materials science aim to overcome these obstacles and unleash the full potential of PMCs across diverse applications.

Modern synthetic fiber-reinforced composites are thought to be less susceptible to fatigue than metallic materials, but it is unavoidable that some properties may deteriorate over time. The theory currently used to predict the lifespan of conventional materials cannot be directly applied to composite materials. An accurate life forecast of composite

structural components under fatigue loading circumstances is essential for design engineers. The stress versus the number of cycles to failure (S–N curve) results are the prerequisite for the macroscopic or microscopic fatigue life prediction models. Localized damage accumulation, such as matrix cracking, fiber-matrix debonding, delamination, fiber rotation, buckling, and other phenomena, is quantified by microscopic models until final breakage [22]. To make more accurate forecasts, models correlate these damage metrics and their growth with the fatigue lifecycle. Macroscopic life prediction, however, does not consider damage mechanisms or its expansion under continuous cyclic loading. Macroscopic Prediction is based on probabilistic, empirical, theoretical, or experimental analysis, including modified S–N curves, residual strengths, stiffness, CLDs, and S–N curves for varied R ratios. For effective life prediction, numerous researchers have recently used genetic algorithms, neuro-fuzzy interference, artificial intelligence, rain flow approaches, artificial neural networks, etc. [23, 24].

As the safe life envelopes fluctuate with fiber orientation, adopting multidirectional laminates in structural applications to decrease anisotropy made the Prediction considerably more challenging. The CLD is a projection of the ultimate tensile strength (UTS) and ultimate compressive strength (UCS) results generated by linearly interpolating the available S–N curves [25]. It is a fatigue life prediction tool that can forecast the safe life envelope and S–N curve for any stress ratio or stacking sequence while saving time and money. The mean (m) and alternating stress (a) sensitivities are considered in this combined plot with UTS, UCS, and S–N curve data. The most straightforward Goodman diagram was the earliest fatigue analysis tool primarily utilized for conventional materials [26]. The anisotropic laminate, however, was not symmetrical about the completely reversed stress ratio, or $R = -1$, due to its differing UTS and UCS. Like the Goodman approach, even the CLD points (pair of mean and amplitude stresses) were not along a straight line. However, the asymmetric shifted, and inclined Goodman diagrams ideally addressed the static strength nonlinearity by repositioning the peak with respect to the zero-mean axis. A significant innovation that separated the diagram into subintervals was the half-spider web-shaped piecewise defined linear CLD diagram [27–29]. A nonlinear interpolation method and a piecewise-defined function were used in an asymmetric and shifted Gerber diagram with a parabolic envelope. The CLD discussed up to this point discussed peak shifting to the right or left, but the trend was unsolved before Kawai and colleagues developed the groundbreaking Anisomorphic CLD [30, 31]. They defined a characteristic stress ratio termed critical stress ratio (CSR) (χ), where alternating stress acquires the most considerable possible value for any arbitrary N_f . CSR was the ratio of compressive to tensile strength, where (UCS < 0) and (UTS > 0). The UTS/UCS of

any laminate determines whether the peak shifts to the left (UTS < UCS) or right (UTS > UCS) of the zero-mean line.

While these nonlinear CLDs can be formulated using any S–N curves and static data as input, linear CLDs require many S–N curves and static data as input. This saves time, work, and money, but it might not be appropriate for a certain stacking and produce subpar predictions. Modern laminate curing procedures and improved fiber manufacturing methods, particularly following the advent of prepregs, have significantly changed the properties of laminates. To demonstrate the importance of CSR, it is necessary to evaluate further the experimental validity of various nonlinear CLDs for different laminates. This study produced extensive experimental constant amplitude fatigue data for a [+45, –45]_{3S} (CFRP45) laminate. Investigations were conducted into the impact of CSR and its importance in assessing the life prediction accuracy of various nonlinear CLDs available in the literature.

Experimental

IMA/ M21 carbon fiber epoxy prepreg was used to manufacture the [+45, –45]_{3S} orientation carbon fiber reinforced polymer (CFRP) composite laminate, which was autoclave-cured at 180° C with a heating rate of 2° C per minute and a dwell time of 120 min. The laminate is termed CFRP45 further, and during layup, prepreg sheets were meticulously organized in alternate directions of +45° and –45° to ensure they were stacked in the correct orientation and produced the best possible mechanical properties. Next, the layup composite structure was placed into a vacuum bag with 1 bar pressure and sealed to remove air, consolidate the layers, and promote uniform resin distribution while minimizing voids. Then, the vacuum-bagged composite laminate was subjected to 180° C heat and 7 bar pressure in an autoclave, initiating the cross-linking of the epoxy matrix and solidifying the composite structure. This controlled curing process ensured the formation of a strong and durable composite material with consistent mechanical properties. The basic properties of the IMA/M21 prepreg are attached to Table 1. The average fiber volume fraction and thickness of the sixteen-layered, 300 × 450 mm laminate were 59% and

Table 1 Physical and mechanical properties of IMA/M21 prepreg

IMA carbon fiber		M21 epoxy matrix	
Tensile strength	6.067 MPa	Flexural yield strength	147 MPa
Tensile modulus	297 GPa	Flexural modulus	3.50 GPa
Density	1.79 g/cm ³	Density	1.28 g/cc
Filament count	12,000	Flexural strain at yield	5%
Filament diameter	5.1 microns	Curing temperature	180° C

3.1 mm, respectively. The static and fatigue test specimens were made with a diamond cutter, and rectangular glass fiber tabs were attached to both ends with Araldite (Epoxy: AV-138, Hardener: HY-998). The end tabs were meticulously trimmed to be close to the gauge length to lessen the effects of tabbing tension.

The static tensile and compressive tests were carried out with a servo-hydraulic universal testing machine, as shown in Fig. 1 (Make: Instron, Model: 8802), following ASTM standards D3039 and D3410, respectively. A crosshead speed of 1 mm/min was employed per standard. Then, room temperature load-controlled constant amplitude fatigue tests were carried out at 2 Hz. Experimentally produced fatigue stress ratios include Tension–Tension (T-T) 0.1 and 0.5, Tension–Compression (T-C) – 1, and Compression–Compression (C–C) 5 stress ratios. The tests were run up to 10^6 cycles, or until failure, and were referred to as runout samples. At least three samples were evaluated to verify the fatigue life at a specific stress level. Figure 2 displays a detailed layout of the specimen geometry and a picture of the specimen utilized in static and fatigue tests [18, 20, 30, 31].

Results and Discussion

Tensile and Compression Test

Tensile and compressive tests on the CFRP45 laminate were performed at room temperature with a 1 mm/min

crosshead speed. It was discovered that the UTS and UCS were 270 ± 10 and 168 ± 7 MPa, respectively. As previously reported, the results showed a nonlinear stress–strain response attributed to stress relaxation caused by fiber rotation and orientation [32–35]. These values were also used to calculate fatigue stress levels and formulate nonlinear CLDs. The CSR was calculated as $\chi = UCS/UTS = -0.64$.

Constant Amplitude Fatigue and S–N Curve

The CFRP45 CFRP laminate’s experimental constant amplitude fatigue data under T–T ($R=0.1$ and 0.5), T–C ($R = -1$ and χ), and C–C ($R=5$) loading was generated. The plot between σ_{max} and N_f is shown in Fig. 3, where the arithmetic mean of at least three comparable fatigue life data corresponding to five stress levels was plotted for all R ratios. The estimated Basquin’s constants, i.e., fatigue strength coefficient (FSC, f) and fatigue strength exponent (FSE, b), are shown in Table 2. The solid line shows the S–N curve was fitted using Basquin’s law according to Eq. 1 [22]. These constants are useful in the mathematical computation of the required N_f or equivalent for any stress ratio.

$$\sigma = \sigma'_f (N_f)^b \tag{1}$$

The UTS/UCS lifespan typically ranged between 30–80%. The lower positioning of the T-T S–N curve at $R=0.1$ compared to $R=0.5$ confirms the previously proven phenomenon

Fig. 1 Fatigue experimental setup

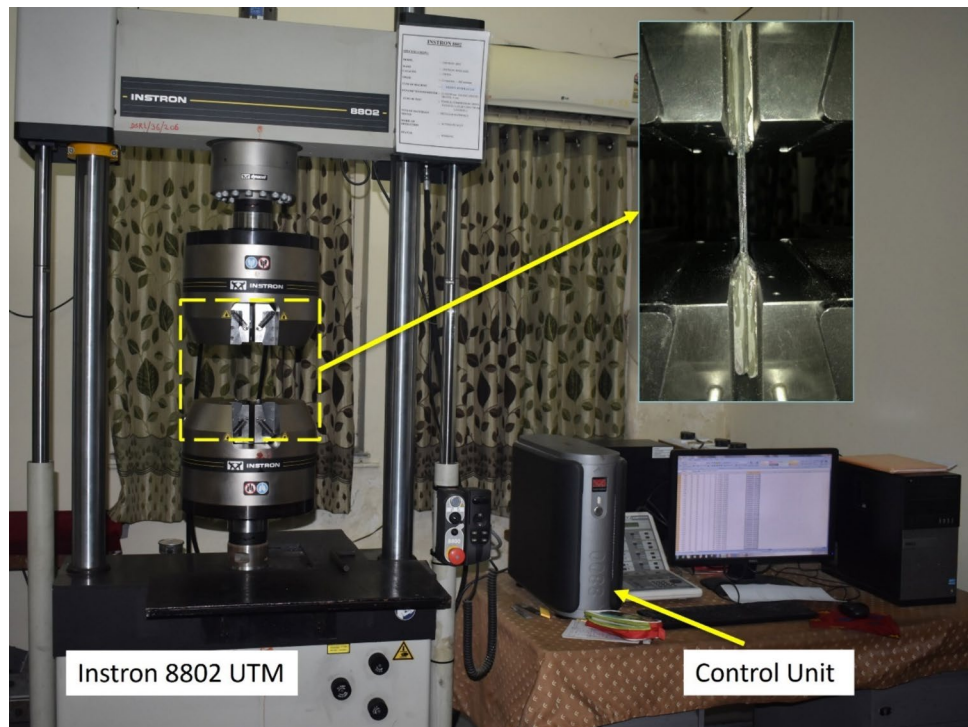


Fig. 2 CFRP45 static and fatigue test specimen geometry and actual test specimen

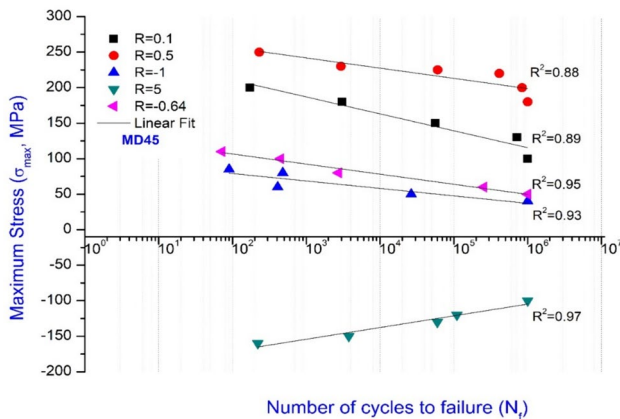
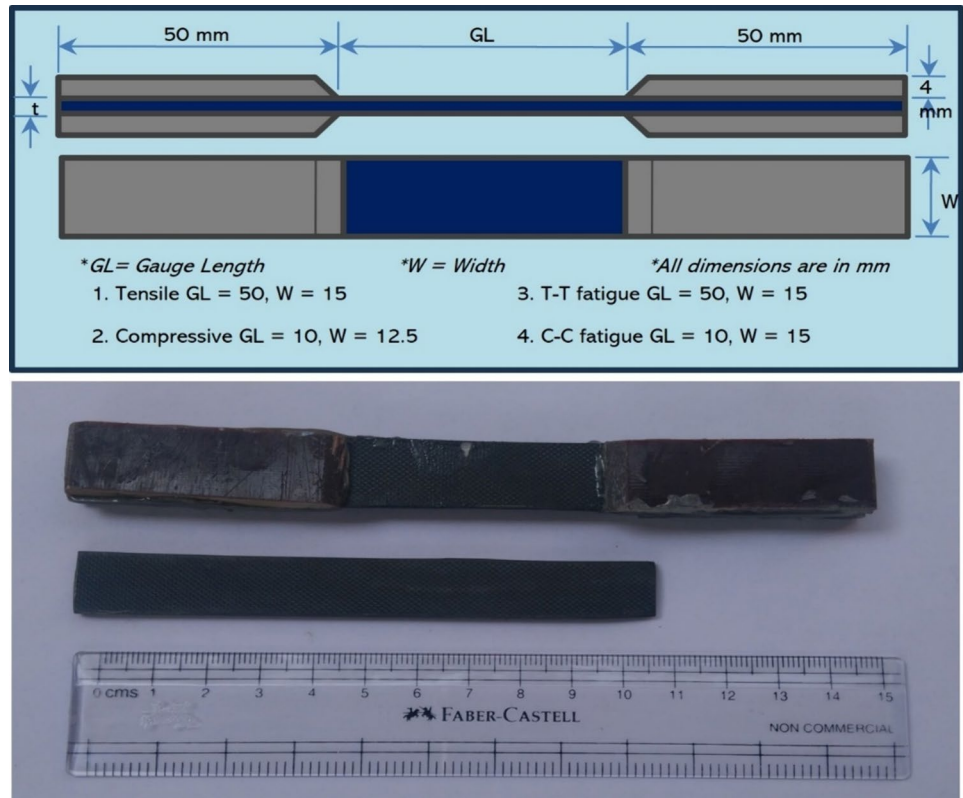


Fig. 3 Constant amplitude S–N curve for CFRP45 laminate

Table 2 Experimental Basquin’s constants of CFRP45 laminate

Stress ratio (R)	σ'_f (FSC), MPa	b (FSE)
0.1	302	– 0.0800
0.5	339	– 0.0459
– 1	140	– 0.0907
5	181	– 0.0432
– 0.64	163	– 0.0805

that the higher the stress range ($\sigma_{max} - \sigma_{min}$), the lower the fatigue life will be [36, 37]. The fact that the slope of 0.1 is steeper than that of 0.5 further supports the effect of mean stress and stress range in T-T loading. The $R = -1$ S–N curve with the steepest slope and a 20–50% lifespan of UCS was the most critical. The S–N curves indicate that T-C loading caused damage more effectively and sensitively than T-T or C–C loading [38].

Constant Life Diagrams

The CLD determines a safe stress envelope within which the composite laminate may withstand more than a specific number of cycles with constant amplitude. CLD can be linear or nonlinear to the alternating stress axis based on interpolation technique or fitting equations. Asymmetric CLDs have distinct UTS and UCS values, while symmetric CLDs have the same values. With CFRP45 laminate having different UTS and UCS values, a few asymmetric nonlinear CLDs from the literature were analyzed in the following sections. The basic Goodman approximation assumes that the largest amplitude stress lies at zero mean stress, i.e., in the completely reversed stress ratio ($R = -1$). The current experimental results observed the highest alternating stress for CSR rather than $R = -1$. This experimental shift of the

highest alternating stress to the left or right of $R = -1$ is called radial peak shift. Numerous researchers documented this radial peak shift [39–46], but Kawai et al. recently defined the shift’s quantification [30, 31].

$$-\frac{\sigma_a - \sigma_a^{R=-1}}{\sigma_a^{R=-1}} = \left(\frac{\sigma_m}{UTS}\right)^2, (0 \leq \sigma_m \leq UTS)$$

$$-\frac{\sigma_a - \sigma_a^{R=-1}}{\sigma_a^{R=-1}} = \left(\frac{\sigma_m}{UCS}\right)^2, (UCS \leq \sigma_m < 0)$$
(2)

Nonlinear Asymmetric CLDs

Researchers have focused on modified nonlinear Goodman or Piecewise diagrams, which are more precise, practical, and time-saving. When using a particular nonlinear analytical function, parabolic or bell-shaped nonlinear CLDs were usually plotted with fewer input nodes. For the current CFRP45 experimental data, a few CLDs from the literature were plotted, and the accuracy was checked.

Asymmetric Gerber CLD

Initially, the nested parabolic-shaped asymmetric Gerber diagram was plotted using a Piecewise-defined parabolic function in Eq. 2, where σ_a = amplitude stress and σ_m = mean stress [47]. According to this equation, the peak will appear at $R = -1$, and the underlying equation will be chosen based on a lower UTS or UCS value. The Gerber diagram derives the T-T, T-C, and C-C zones with a single equation. Currently, for CFRP45 laminate with UCS lower than UTS, the 2nd part of Eq. 2 was employed to plot the Gerber diagram, as shown in Fig. 4, with input stress ratio $R = -1$. The figure demonstrates that the overall prediction accuracy of this CLD for $R = 0.1, 0.5$, and 5 was inferior if compared with the experimental data projected in the S–N curve.

Shifted Gerber CLD

Gerber CLD did not address the experimental peak lying about non-zero mean stress. Later, this peak shift was addressed by shifted Gerber parabolic CLD where traditional Gerber CLD shifts to a non-zero mean (χ) following a Piecewise-defined function as given in Eq. 3. Here, σ_M is a constant denoting the mean of UTS and UCS whereas σ_A is a function N_f . The parabola with two different foci in the tension and compression zone was smoothly connected along with an unknown stress ratio (χ), as shown in Fig. 5. This R ratio was conveyed as Eq. 4 without any quantification till Kawai and coworker solved this recently [30, 31]. The prediction accuracy of the shifted Gerber CLD was comparatively more acceptable than traditional Gerber CLD, but the consideration of the unknown stress ratio was unsolved.

$$-\frac{\sigma_a - \sigma_A}{\sigma_A} = \left(\frac{\sigma_m - \sigma_M}{UTS - \sigma_M}\right)^2, \sigma_M \leq \sigma_m \leq \sigma_T$$

$$-\frac{\sigma_a - \sigma_A}{\sigma_A} = \left(\frac{\sigma_m - \sigma_M}{UCS - \sigma_M}\right)^2, \sigma_C \leq \sigma_m < \sigma_M$$
(3)

$$\chi = \frac{(\sigma_M - \sigma_A)}{(\sigma_M + \sigma_A)}$$
(4)

Fig. 4 Asymmetric Gerber CLD for CFRP45 laminate

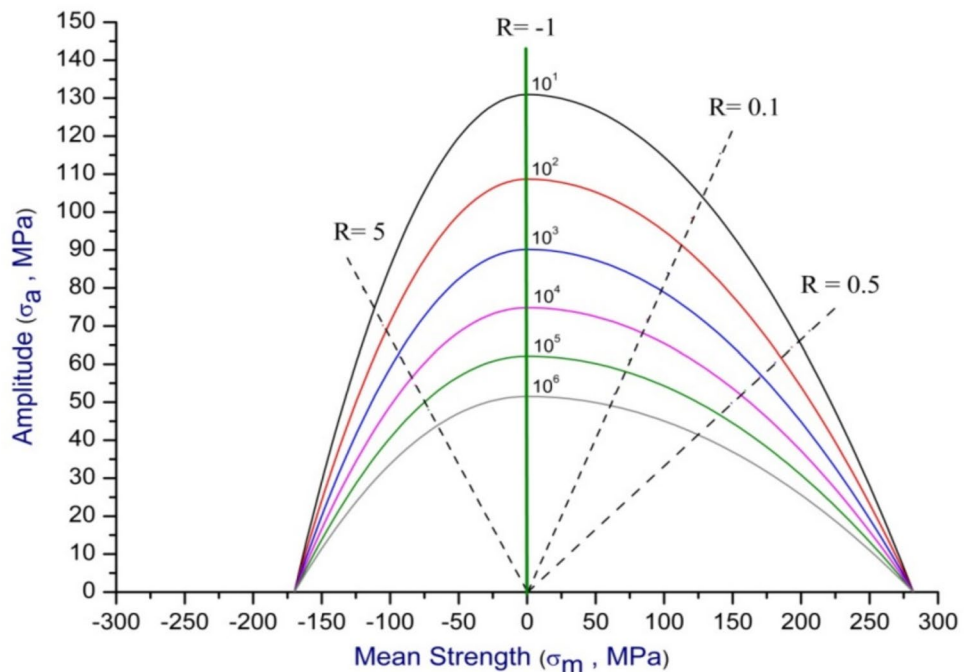
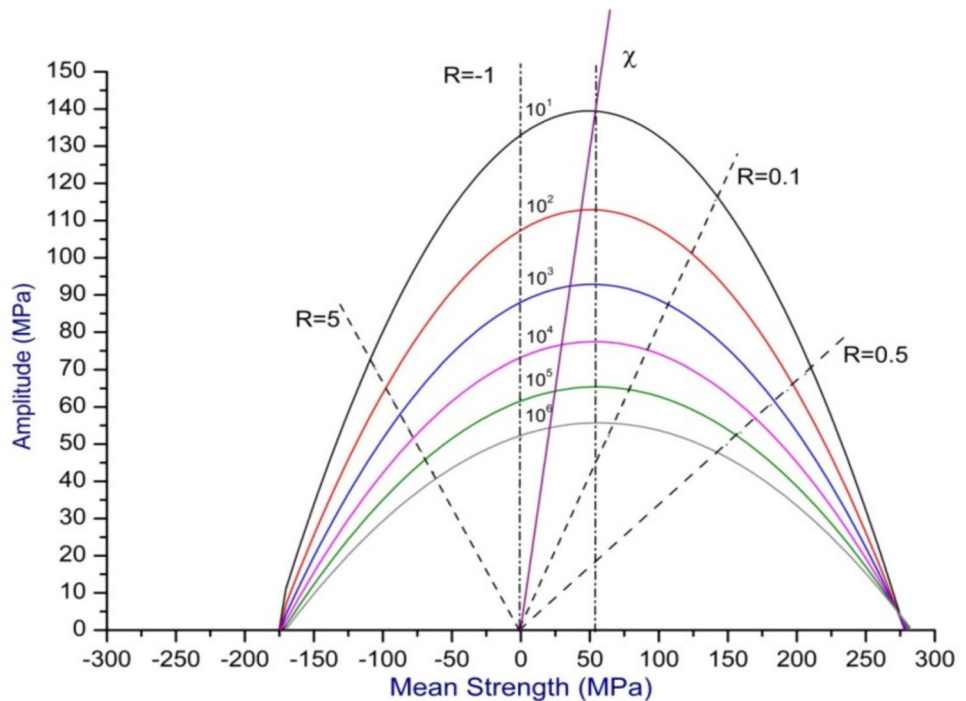


Fig. 5 Shifted asymmetric Gerber CLD for CFRP45 laminate



Where, $\sigma_M = \frac{UTS + UCS}{2}$

The shifted symmetric Gerber diagram showed acceptable prediction accuracy for carbon/Kevlar hybrid composites [40] and carbon fiber composites [43, 44]. The innovative bell-shaped CLD and inclined Gerber diagram were also developed because of this shifted Gerber diagram, and their correctness has been examined in the literature. Much research has been done on the bell-shaped diagram for different CFRP and GFRP composite laminates [22, 25]. Using nonlinear regression and material functions based on fatigue data, this method is complicated. This CLD can be extended mathematically to fit the bell-shaped CFL diagram. Eventually, Kawai and colleagues created a unique anisomorphic nonlinear CLD employing all these databases.

Anisomorphic Nonlinear CLD

The Anisomorphic CLD mathematically described the radial peak shift line as Eq. 5, where χ stands for the CSR. The T-T and C-C fatigue failure modes split the CLD into two halves along this radial line. Equation 6 only requires the CSR S-N curve values, UTS, and UCS to create the tension and compression side curves. In this case, UCS is negative, UTS is positive, the exponent " $\psi_{(R=\chi)}$ " represents the function of N_f , and " σ_B^χ " stands for a constant reference strength to be found for the CSR. The range of $(2 - \psi_{(R=\chi)})$ in Eq. 6 is constrained between one and two, i.e., $1 \leq 2 - \psi_{(R=\chi)} \leq 2$. This is because the variable exponent " $\psi_{(R=\chi)}$ "

always resides between zero and one, i.e., $0 \leq \psi_{(R=\chi)} \leq 1$. This CLD produces nested parametric curves whose shape gradually changes from a straight line to a parabola as fatigue life increases [48].

$$\frac{\sigma_a}{\sigma_m} = \frac{1 - \chi}{1 + \chi} \tag{5}$$

$$\frac{\sigma_a - \sigma_a^{R=\chi}}{\sigma_a^{R=\chi}} = \begin{cases} \left(\frac{\sigma_m - \sigma_m^{R=\chi}}{UTS - \sigma_m^{R=\chi}} \right)^{2 - \psi_{(R=\chi)}}, & (\sigma_m^{R=\chi} \leq \sigma_m \leq UTS) \\ \left(\frac{\sigma_m - \sigma_m^{R=\chi}}{UCS - \sigma_m^{R=\chi}} \right)^{2 - \psi_{(R=\chi)}}, & (UCS \leq \sigma_m \leq \sigma_m^{R=\chi}) \end{cases} \tag{6}$$

Where, $\psi_{(R=\chi)} = \frac{\sigma_{max}^{R=\chi}}{\sigma_B^{R=\chi}}$

The same equation was used to create four different CLDs using different experimental CFRP45 stress ratios, namely $R = 0.1, 0.5, -1$, and 5 , before creating the suggested CLD utilizing the CSR data, as shown in Fig. 6a-d. For the remainder of experimental S-N curves, the prediction accuracy of the $R = 0.5$ and $R = 5$ Anisomorphic CLD was less than optimal. On the other hand, $R = 0.1$ and $R = -1$ demonstrated superior prediction accuracy for the T-T and C-C zones, respectively. Notably, for $R = 5$, the $R = 0.1$ anisomorphic CLD's prediction accuracy was close to the experiments' outcomes. The optimal stress ratio was $R = -1$ based on the CLD peak and overall Prediction.

The associated radially and correlated σ_{Mean} and $\sigma_{Amplitude}$, as given in Eq. 5-6, were resolved using the

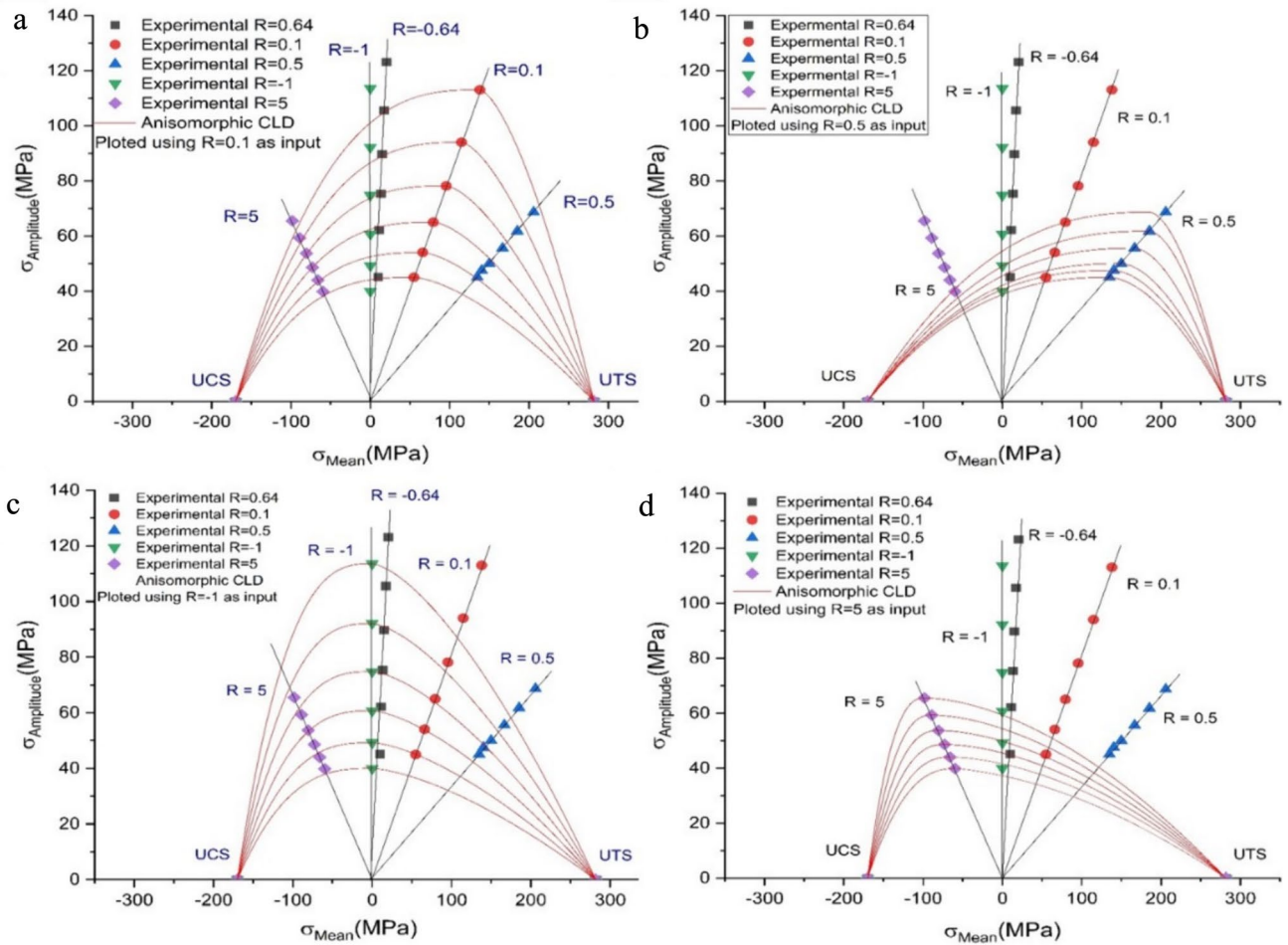


Fig. 6 CFRP45 anisomorphic CLDs formulated with input stress ratios (R) of **a** 0.1, **b** 0.5, **c** -1, and **d** 5

anisomorphic CLD diagram, as shown in Fig. 7 [48]. This represents the CLD after considering experimental fatigue data points of CSR ($\chi = -0.64$). The curve’s apex has shifted to the right, which also denotes an ultimate tensile-dominated failure of the CFRP45 laminate. Any stress ratio within the life envelope can be predicted using the plotted CLD. The anisomorphic CLD plotted using critical stress as input offered the highest accuracy out of all the experimental CLDs.

Table 3 displays the inaccuracy % between experimental and anamorphic CLD prediction. The T-T S-N curves have errors below 10%. However, the C-C and fully reversed stress ratios exhibited close to 20% inaccuracy. As the CFRP45 failed under the dominance of tensile loading, the prediction in the T-T domain was better than that in the C-C domain. Researchers designed the three-segment anisomorphic CLD with an additional input node to broaden the anisomorphic CLD and address this problem of poor prediction based on the mode of failure [49].

This study addresses a crucial gap in knowledge by highlighting the limitations of linear CLDs and the importance of CSR in accurately predicting the fatigue life of composite laminates. While nonlinear CLDs offer a streamlined approach requiring fewer input parameters, linear CLDs may yield sub-par predictions, especially for complex laminate configurations. The evolution of laminate curing procedures and fiber manufacturing methods necessitates a reassessment of CLD validity across different laminates. Focused on a $[+45, -45]_{3S}$ laminate, the study generates extensive experimental fatigue data to evaluate the impact of CSR on the predictive accuracy of various nonlinear CLDs, bridging the gap between theory and practical application in composite materials engineering.

Conclusions

Nonlinear CLDs are a practical tool for estimating the fatigue life of composite materials with various orientations

Fig.7 CFRP45 anisomorphic CLD plotted using static and CSR data

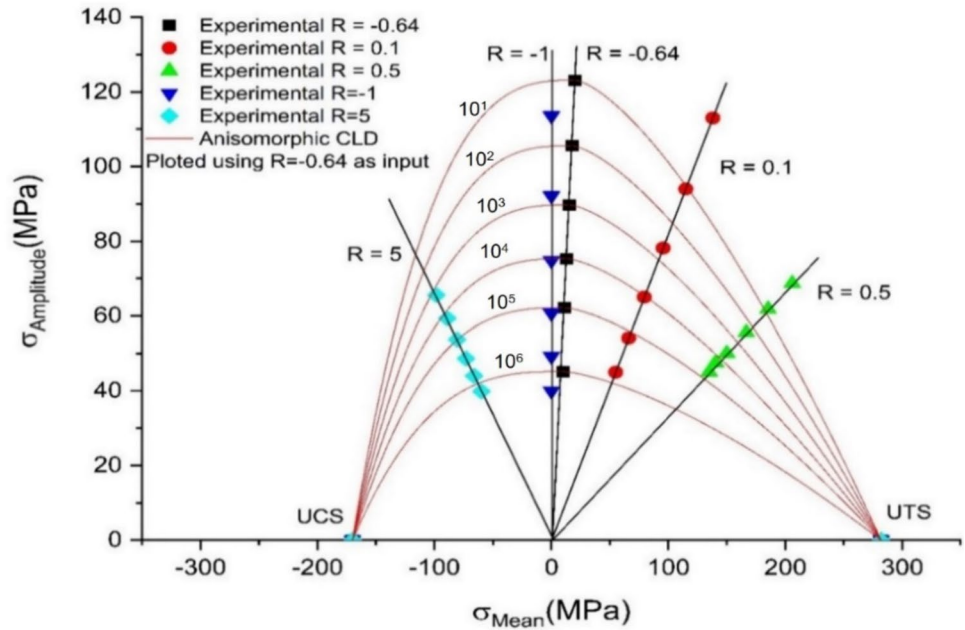


Table 3 Error in experimental and anamorphic prediction

Stress ratio (R)	Experimental and anisomorphic prediction error (%)	
	Mean stress	Amplitude stress
0.5	8.9	9.7
0.1	6.6	6.5
- 1	0	17.7
5	19.9	19

and stacking configurations. This study specifically investigated the predictive accuracy of several nonlinear CLDs for a laminated Carbon Fiber Reinforced Polymer composite with $[+45, -45]_{3S}$ layup. Comparing experimental findings with anisomorphic CLD projected values revealed exciting insights. Experimental and theoretical error percentages were lower for T-T stress ratios but higher for C-C stress ratios. Introducing a transitional zone, i.e., critical stress ratio in the anisomorphic CLD, notably enhanced forecast accuracy. This innovative approach simplifies the predictive process and minimizes the required testing. By integrating a transitional zone, the anisomorphic CLD effectively mitigates mean stress sensitivity and offers accurate predictions with minimal input data, primarily comprising Ultimate Tensile Strength (UTS), Ultimate Compressive Strength (UCS), and CSR. Implementing these nonlinear CLDs can streamline labor-intensive and costly testing processes, saving valuable resources like time, effort, and financial investments. Future research can lead to refining and validating

CLDs across different composite materials and configurations and exploring the impact of environmental factors on predictions. Overall, nonlinear CLDs hold promise for streamlining testing procedures and improving efficiency in composite material design and evaluation.

Acknowledgements The authors sincerely thank the Director, VNIT, and the Head of the Department, Metallurgical and Materials Engineering, VNIT, Nagpur, for providing testing facilities and support.

Funding No funding was received.

Data Availability Statement The data used to support the findings of this study are available from the corresponding author upon request.

Declarations

Conflict of interest The authors declare that they have no known competing financial interests or personal relationships that could have appeared to influence the work reported in this paper.

References

1. J. Zhang, G. Lin, U. Vaidya, H. Wang, Past, present and future prospective of global carbon fibre composite developments and applications. *Compos. B Eng.* **250**, 110463 (2023)
2. N. Mohammed, P. Palaniandy, F. Shaik, B. Deepanraj, H. Mewada, Statistical analysis by using soft computing methods for seawater biodegradability using ZnO photocatalyst. *Environ. Res.* **227**, 115696 (2023)
3. A. Behera, M.M. Thawre, A. Ballal, P. Babrekar, P. Vaidya, S. Vijetha, et al. Effect of moisture content and fiber orientation on the mechanical behavior of GFRP composites (2021)
4. M.A. Syed, Z.S. Al-Shukaili, F. Shaik, N. Mohammed, Development and characterization of algae based semi-interpenetrating

- polymer network composite. Arab. J. Sci. Eng. **47**, 5661–5669 (2022)
5. A. Behera, A. Vishwakarma, M.M. Thawre, A. Ballal, Effect of hygrothermal aging on static behavior of quasi-isotropic CFRP composite laminate. Compos. Commun. **17**, 51–55 (2020)
 6. N. Mohammed, P. Palaniandy, F. Shaik, H. Mewada, Statistical modelling of solar photocatalytic biodegradability of seawater using combined photocatalysts. J. Inst. Eng. (India) Ser. E **104**, 251–267 (2023)
 7. A. Behera, M.M. Thawre, A. Ballal, Effect of matrix crack generation on Fatigue life of CFRP multidirectional laminates. Mater. Today Proc. **5**, 20078–20084 (2018)
 8. N. Mohammed, P. Palaniandy, F. Shaik, H. Mewada, Experimental and computational analysis for optimization of seawater biodegradability using photo catalysis. IIUM Eng. J. **24**, 11–33 (2023)
 9. A. Behera, N.K. Bhoi, M.M. Thawre, A. Ballal, D. Das, Quantification of hygrothermal aging-induced interfacial debonding of carbon fiber/epoxy composites at nano-to-micrometer length scales. J. Compos. Mater. **57**, 4637–4647 (2023)
 10. A. Behera, M.M. Thawre, A. Ballal, Hygrothermal aging effect on physical and mechanical properties of carbon fiber/epoxy cross-ply composite laminate. Mater. Today Proc., **28** (2019)
 11. A. Behera, J. Dehury, M.M. Thawre, A comparative study on laminated and randomly oriented Luffa-Kevlar Reinforced hybrid composites. J. Nat. Fibers **16**, 237–244 (2019)
 12. A. Vishwakarma, A. Behera, M.M. Thawre, A.R. Ballal, Effect of thickness variation on static behaviour of carbon fiber reinforced polymer multidirectional laminated composite. Mater. Res. Express **6**, 115312 (2019)
 13. A. Behera, J. Dehury, B.P. Rayaguru, The consequence of SiC filler content on the mechanical, thermal, and structural properties of a Jute/Kevlar reinforced epoxy hybrid composite. SILICON **15**, 6509–6519 (2023)
 14. A. Purohit, J. Dehury, L.N. Rout, S. Pal, A novel study of synthesis, characterization and erosion wear analysis of glass-jute polyester hybrid composite. J. Inst. Eng. (India) Ser. E **104**, 1–9 (2023)
 15. A. Purohit, G. Gupta, P. Pradhan, A. Agrawal, Development and erosion wear analysis of polypropylene/Linz-Donawitz sludge composites. Polym. Compos. **44**, 6556–6565 (2023)
 16. P. Pradhan, A. Purohit, J. Singh, C. Subudhi, S.S. Mohapatra, D. Rout et al., Tribo-performance analysis of an agro-waste-filled epoxy composites using finite element method. J. Inst. Eng. (India) Ser. E **103**, 339–345 (2022)
 17. A. Purohit, P.T.R. Swain, P.K. Patnaik, Mechanical and sliding wear characterization of LD sludge filled hybrid composites. Mater. Today Proc. **26**, 1654–1659 (2019)
 18. A. Behera, P. Dupare, M.M. Thawre, A. R. Ballal, Effect of fatigue loading on stiffness degradation, energy dissipation, and matrix cracking damage of CFRP [± 45]_{3S} composite laminate. Fatigue Fract. Eng. Mater. Struct. **42** (2019)
 19. J. Dehury, A. Behera, S. Biswas, A study on the mechanical behavior of jute-epoxy laminated composite and its hybrid. Mater. Sci. Forum **978**, 250–256 (2020)
 20. A. Behera, P. Dupare, M.M. Thawre, A. Ballal, Effects of hygrothermal aging and fiber orientations on constant amplitude fatigue properties of CFRP multidirectional composite laminates. Int. J. Fatigue **136**, 105590 (2020)
 21. A. Behera, M.M. Thawre, A. Ballal, C.M. Manjunatha, D. Krishnakumar, S. Chandankhede, A modified piecewise linear constant life diagram for fatigue life prediction of carbon fiber/polymer multidirectional laminates. Polym. Compos. **44**, 1360–1370 (2023)
 22. B. Harris, *Fatigue in Composites* (Woodhead Publishing, Cambridge, 2003)
 23. G. Galanopoulos, D. Milanoski, N. Eleftheroglou, A. Broer, D. Zarouchas, T. Loutas, Acoustic emission-based remaining useful life prognosis of aeronautical structures subjected to compressive fatigue loading. Eng. Struct. **290**, 116391 (2023)
 24. Z. Liang, X. Wang, Y. Cui, W. Xu, Y. Zhang, Y. He, A new data-driven probabilistic fatigue life prediction framework informed by experiments and multiscale simulation. Int. J. Fatigue **174**, 107731 (2023)
 25. G.P. Sendeckyj, Constant life diagrams—a historical review. Int. J. Fatigue **23**, 347–353 (2001)
 26. J. Goodman, *Mechanics Applied to Engineering*, London (Green & Co., Longmans, 1899)
 27. M.H. Beheshty, B. Harris, A constant-life model of fatigue behaviour for carbon fibre composites: the effect of impact damage. Compos. Sci. Technol. **58**, 9–18 (1998)
 28. Z. Hashin, Fatigue failure criteria for unidirectional fiber composites. ASME J. Appl. Mech. **48**, 846–852 (1981)
 29. Z. Hashin, A. Rotem, A fatigue failure criterion for fiber-reinforced materials. J. Compos. Mater. **7**, 448–464 (1973)
 30. M. Kawai, M. Koizumi, Nonlinear constant fatigue life diagrams for carbon/epoxy laminates at room temperature. Compos. Part A **38**, 2342–2353 (2007)
 31. M. Kawai, T. Murata, A modified asymmetric anisomorphic constant fatigue life diagram and application to CFRP symmetric angle-ply laminates, in *Proc 13th US-Japan Conf Compos Mater (CD-ROM)*, Nihon University, Tokyo, 6–7 June 2008, pp. 1–8
 32. Z. Mahboob, I. El Sawi, R. Zdero, Z. Fawaz, H. Bougherara, Tensile and compressive damaged response in Flax fibre reinforced epoxy composites. Compos. Part A Appl. Sci. Manuf. **92**, 118–133 (2017)
 33. S.C. Garcea, Y. Wang, P.J. Withers, X-ray computed tomography of polymer composites. Compos. Sci. Technol. **156**, 305–319 (2018)
 34. M.J. Emerson, K.M. Jespersen, A.B. Dahl, K. Conradsen, L.P. Mikkelsen, Individual fibre segmentation from 3D X-ray computed tomography for characterising the fibre orientation in unidirectional composite materials. Compos. Part A Appl. Sci. Manuf. **97**, 83–92 (2017)
 35. A. Behera, M.M. Thawre, A. Ballal, Failure analysis of CFRP multidirectional laminates using the probabilistic Weibull distribution model under static loading. Fibers Polym. **20**, 2390–2399 (2019)
 36. M. Kawai, *Fatigue Life Prediction of Composite Materials Under Constant Amplitude Loading* (Woodhead Publishing, Cambridge, 2010), pp. 171–219
 37. M. Kawai, S. Saito, Off-axis strength differential effects in unidirectional carbon/epoxy laminates at different strain rates and predictions of associated failure envelopes. Compos. Part A Appl. Sci. Manuf. **40**(10), 1632–1649 (2009)
 38. M. Kawai, A phenomenological model for Off-axis fatigue behavior of unidirectional polymer matrix composites under different stress ratios. Compos. Part A Appl. Sci. Manuf. **35**(7–8), 955–963 (2004)
 39. M. P. Ansell, I. P. Bond, P. W. Bonfield, Constant life diagrams for wood composites and polymer matrix composites, in *Proc 9th Int Conf Compos Mater (ICCM9)*, Madrid, V, pp. 692–9 (1993)
 40. T. Adam, G. Fernando, R.F. Dickson, H. Reiter, B. Harris, Fatigue life prediction for hybrid composites. Int. J. Fatigue **11**(4), 233–237 (1989)
 41. T. Adam, N. Gathercole, H. Reiter, B. Harris, Fatigue life prediction for carbon fibre composites. Adv. Compos. Lett. **1**, 23–26 (1992)
 42. M.H. Beheshty, B. Harris, T. Adam, An empirical fatigue-life model for high-performance fibre composites with and without impact damage. Compos. Part A. **30**, 971–987 (1999)

43. N. Gathercole, H. Reiter, T. Adam, B. Harris, Life prediction for fatigue of T800/5245 carbon-fibre composites: I constant-amplitude loading. *Fatigue* **16**, 523–532 (1994)
44. B. Harris, H. Reiter, T. Adam, R.F. Dickson, G. Fernando, Fatigue behaviour of carbon fibre reinforced plastics. *Composites* **21**(3), 232–242 (1990)
45. B. Harris, N. Gathercole, J.A. Lee, H. Reiter, T. Adam, Life-prediction for constant-stress fatigue in carbon-fibre composites. *Phil. Trans. R. Soc. Lond.* **A355**, 1259–1294 (1997)
46. M. Kawai, M. Koizumi, Nonlinear constant fatigue life diagrams for carbon/epoxy laminates at room temperature. *Compos. Part A Appl. Sci. Manuf.* **38**, 2342–2353 (2007)
47. W.Z. Gerber, Bestimmung der zulässigen Spannungen in Eisen-constructionen (calculation of the allowable stresses in iron structures)'. *Z. Bayer Archit. Ing.-Ver.* **6**(6), 101–110 (1874)
48. M. Kawai, *Fatigue Life Prediction of Composite Materials Under Constant Amplitude Loading*, 2nd edn. (Woodhead Publishing, Sawston, 2020), p.425
49. M. Kawai, T. Murata, A modified asymmetric anisomorphic constant fatigue life diagram and application to CFRP symmetric angle-ply laminates, *Proc 13th US Japan Conf Compos Mater (CD-ROM)*, Nihon University, Tokyo, 6–7 June 1–8 (2008)

Publisher's Note Springer Nature remains neutral with regard to jurisdictional claims in published maps and institutional affiliations.

Springer Nature or its licensor (e.g. a society or other partner) holds exclusive rights to this article under a publishing agreement with the author(s) or other rightsholder(s); author self-archiving of the accepted manuscript version of this article is solely governed by the terms of such publishing agreement and applicable law.